Analysis and Applications of "Microstrip-Loaded Inset Dielectric Waveguide" (Mig)

Tullio Rozzi, *Fellow, IEEE* Antonio Morini, and Giampiero Gerini

Abstract—**We investigate analytically and experimentally the properties of mig (microstrip inset guide) [1], highlighting its features with respect to microstrip and its applications to antenna circuitry. The method used in the analysis is the transverse resonance diffraction (TRD) method in the space domain [2]. We discuss dispersion of the first three modes, field distribution, characteristic impedance and losses of the fundamental mode. Finally, we report the experimental antenna characteristics of an array of longitudinal strips, designed as a cascade of mig sections alternate to idg (inset dielectric guide) sections, showing good gain input match and pure polarization.**

I. Introduction

INSET dielectric guide (idg) [1], [2] is constituted by a dielectric filled groove on a ground plane. Microstrip-loaded inset dielectric guide is obtained by placing a longitudinal strip on the air dielectric interface of an idg (Fig. 1). This guide supports a fundamental mode without cutoff, analogous to the fundamental mode of ordinary open microstrip, plus a spectrum of modes similar to that of idg. Mig offers an accessible interface (i.e., the air-dielectric interface, that presents two conductors on the same plane, as in coplanar guide) for planar technologies. In particular, the realization of a short circuit in mig does not require drilling a hole in the dielectric substrate. It is important to note however that the side walls of the groove prevent the propagation of a surface mode, which often affects the performance of microstrip and coplanar guide circuits at the cost of a slightly more complex fabrication. In addition, integration with other planar structures, such as microstrip, coplanar asymmetrical slotline etc., seems quite simple and this is particularly important in integrating feeds and planar antennas [3]. In fact mig can be a feeder for idg antenna and the antenna itself may be studied as a cascade of idg sections alternate to mig sections (Fig. 2).

II. Analysis

We analyze the mig guide by the TRD method [2], by considering odd modes only. These comprise the fundamental-quasi TEM-mode and imply a magnetic wall in $x = 0$ plane. The continuity of the tangential EM field at the air-dielectric interface ($y = 0$ plane, with reference to the Fig. 1) produces the following vector integral equation:

$$\begin{bmatrix} \tilde{Y}_{11}\tilde{Y}_{12} \\ \tilde{Y}_{21}\tilde{Y}_{22} \end{bmatrix} \begin{bmatrix} E_x(x, 0) \\ \dfrac{a}{\pi} E_z'(x, 0) \end{bmatrix} = 0. \tag{1}$$

The complete expressions of the kernels of the Green's integral operators $\tilde{Y}_{ij}$ of the previous equation are found in analogous manner as in [1]–[3].

It is noted that we use E_z' instead of E_z because it satisfies the same boundary and singular edge conditions as E_x at the interface. This choice also improves convergence of the solution of the integral equation. We solve the integral equation (1) by the Galerkin's method in the space domain. In order to achieve fast convergence, we build in the edge conditions in the solution by expanding the unknown field in terms of a set of orthonormalized functions weighted by an appropriate singular function. In particular, the presence of the 0°-edge ($x = w/2$) im-

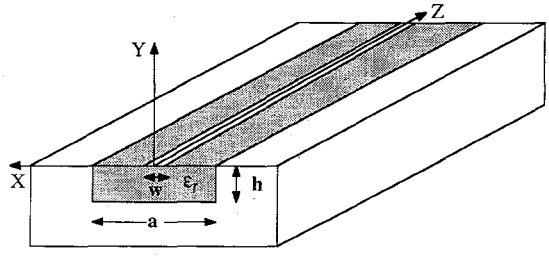

Fig. 1. Microstrip loaded inset guide.

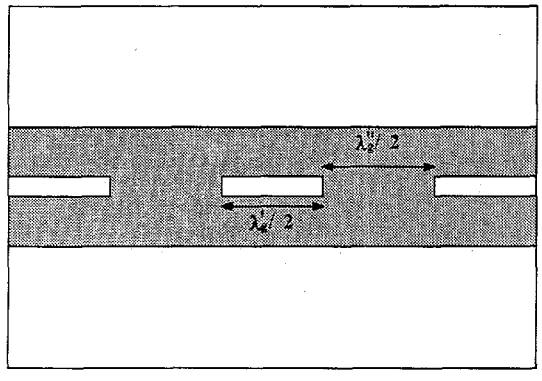

Fig. 2. Horizontally polarized array.

Manuscript received October 8, 1990; revised May 29, 1991.

The authors are with the Dipartimento di Elettronica ed Automatica, Università di Ancona, Via Brecce Bianche, 60131 Ancona, Italy.

IEEE Log Number 9104766.

plies a behavior of $r^{-1/2}$-type and the 270°-edge ($x = a/2$) of $r^{-1/3}$-type (Fig. 3). Hence, by choosing a weight function $W(x) = (1 - 2x/a)^{-1/3}(2x/w - 1)^{-1/2}$, we satisfy automatically the edge conditions.

The set of basis functions that are orthonormalized with respect to this weight function are the Jacobi's polynomials G_n of order $(\frac{1}{6}; \frac{1}{2})$ [5], [6]. Therefore, we express the E-field as

$$E_x(x, o) = \frac{1}{\sqrt[3]{1 - \left(\frac{2x}{a}\right)}\sqrt{\left(\frac{2x}{w}\right) - 1}} \cdot \sum_{n=0,1\cdots}^{N_x - 1} X_n f_n\left(\frac{2x - w}{a - w}\right). \quad (2a)$$

$$\frac{a}{\pi}E_z'(x, o) = \frac{a}{\pi}\frac{d}{dx}E_z(x, o) = \frac{1}{\sqrt[3]{1 - \left(\frac{2x}{a}\right)}\sqrt{\left(\frac{2x}{w}\right) - 1}} \cdot \sum_{n=1,2\cdots}^{N_z} Z_n f_n\left(\frac{2x - w}{a - w}\right) \quad (2b)$$

where

$$f_n(z) = \frac{G_n(\frac{1}{6}; \frac{1}{2}; z)}{N_n}$$

$$N_n = \sqrt{\left(\frac{a}{2}\right)^{1/3}\left(\frac{w}{2}\right)^{1/8}\left(\frac{a - w}{2}\right)^{1/6}\frac{n!\,\Gamma(n + \frac{1}{2})\Gamma(n + \frac{1}{6})\Gamma(n + \frac{2}{3})}{(2n + \frac{1}{6})\Gamma^2(2n + \frac{1}{6})}}.$$

It is noted that the sum in (2b) begins from $n = 1$. The reason is that E_z vanishes at the strip edge ($x = w/2$) and at the groove edge ($x = a/2$), so that E_z' must have zero average in this range. Using the above expanding functions, the matrix elements (i, j) of the discretized admittance operators become

$$j\omega\mu_o[Y_{11}]_{ij} = \sum_{n=1,3\cdots}^{\infty}(\epsilon_r k_o^2 - \beta^2)\frac{\cot q_n h}{q_n}P_{\text{in}}P_{jn} + (\beta^2 - k_o^2)\int_0^\infty \frac{dk_x}{\sqrt{\beta^2 - k_o^2 + k_x^2}} \cdot P_i(k_x)P_j(k_x) \quad \begin{cases} i = 0, 1, \cdots N_x - 1 \\ j = 0, 1, \cdots N_x - 1 \end{cases} \quad (3a)$$

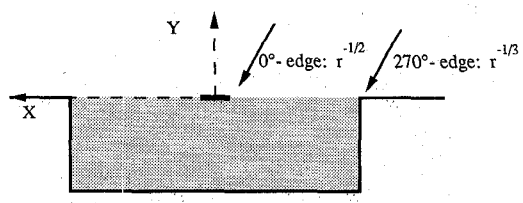

Fig. 3. Transverse section of mig.

and similarly,

$$j\omega\mu_o[Y_{12}]_{ij} = j\beta\left(\frac{\pi}{a}\right)\left(\sum_{n=1,3\cdots}^{\infty}\frac{\cot q_n h}{q_n}P_{\text{in}}P_{jn} - \int_0^\infty \frac{dk_x}{\sqrt{\beta^2 - k_o^2 + k_x^2}}P_i(k_x)P_j(k_x)\right) \quad \begin{cases} i = 0, 1, \cdots N_x - 1 \\ j = 1, 2, \cdots N_z \end{cases} \quad (3b)$$

$$j\omega\mu_o[Y_{22}]_{ij} = \left(\frac{\pi}{a}\right)^2\left(\sum_{n=1,3\cdots}^{\infty}\frac{\cot q_n h}{q_n}\frac{\epsilon_r k_o^2 - \left(\frac{n\pi}{a}\right)^2}{\left(\frac{n\pi}{a}\right)^2} \cdot P_{\text{in}}P_{jn} + \int_0^\infty \frac{dk_x}{\sqrt{\beta^2 - k_o^2 + k_x^2}} \cdot \left(1 - \frac{k_0^2}{k_x^2}\right)P_i(k_x)P_j(k_x)\right) \quad \begin{cases} i = 1, 2, \cdots N_z \\ j = 1, 2, \cdots N_z \end{cases} \quad (3c)$$

$$[Y_{12}]_{ij} = -[Y_{21}]_{ji}$$

where

$$P_i(k_x) = \int_{a/2}^{w/2}\Phi(x, k_x)f_i(x)\,dx$$

$$P_{\text{in}} = \int_{a/2}^{w/2}\Phi_n(x)f_i(x)\,dx \quad (4a)$$

$$\Phi(x, k_x) = \sqrt{\frac{2}{\pi}}\sin(k_x x) \quad \Phi_n(x) = \frac{2}{\sqrt{a}}\sin\left(\frac{n\pi}{a}x\right). \quad (4b)$$

The complete expressions of the Fourier coefficients $P_i(k_x)$, P_{in} are reported in the Appendix. Finally, the integral equation (1) becomes the following matrix equa-

tion:

$$\begin{bmatrix} \underline{\underline{Y}}_{11}(\beta) & \underline{\underline{Y}}_{12}(\beta) \\ \underline{\underline{Y}}_{21}(\beta) & \underline{\underline{Y}}_{22}(\beta) \end{bmatrix} \begin{bmatrix} \underline{X} \\ \underline{Z} \end{bmatrix} = 0. \quad (5)$$

The vanishing of the determinant of the Y matrix in (5) produces the propagation constant β of the guide. The order of the system (5) regards the mig dimensions and the order of the mode we are interested for. In those cases that we analyzed ($1.5 < a/w < 20$), we obtained accurate dispersion curves with a [3 × 3] system. This accuracy cannot be guaranteed with the same order of the system for $a/w > 20$. We must note that so rapid a convergence is a consequence of stationarity of the expression for β/k_o. Typically, a two dimensional vector for $\underline{X}(N_x = 2)$ and a scalar for $\underline{Z}(N_z = 1)$ give good results, as can be seen in Table I. Once β is known, it is possible to solve the system (5), within a normalization constant, which is determined by normalizing the modal power, and to find the field distribution. Fig. 4 shows a typical E-field plot in a cross section. As this is not a variational quantity a somewhat higher order of expansion is required to obtain accurate field plots. An efficient approach, however, is provided by solving the dispersion equation for low order system to obtain β and then utilize this values in (5) with higher values of N_x and N_z in order to determine $\underline{X}$, $\underline{Z}$.

III. Results

All results are obtained for a mig filled by Teflon ($\epsilon_r = 2.08$).

Dispersion Curves and Characteristic Impedance

Fig. 5 shows the dispersion curves for the first three odd modes of the guide ($w = 2$ mm, $h = 10.16$ mm, $a = 22.84$ mm) in the range 0–40 GHz. Fig. 6 shows a comparison, in the monomode range, between theoretical and experimental values of λ_g, measured by a mig resonant cavity 10 cm long. The complete s_{11} and s_{21} experimental data are reported in Fig. 7.

In view of the arbitrariness of the definition of characteristic impedance, we compared the results of three possible definitions: the first by assuming the voltage drop between the strip edge and metal flange, the second between strip center and bottom of the groove, the third, by considering the circuitation of the magnetic field around the strip. Following these three different definitions, we have

$$Z_{ov1} = \frac{V_1^2}{2P} \quad (6a)$$

$$Z_{ov2} = \frac{V_2^2}{2P} \quad (6b)$$

$$Z_{oi} = \frac{2P}{I^2} \quad (6c)$$

TABLE I
TABLE OF CONVERGENCE

Frequency [GHz]	$\beta/k0$ [1 × 1]	$\beta/k0$ [3 × 3]	$\beta/k0$ [7 × 7]
1.0	1.275	1.261	1.262
4.0	1.295	1.276	1.276
8.0	1.336	1.308	1.308
10.0	1.356	1.326	1.325

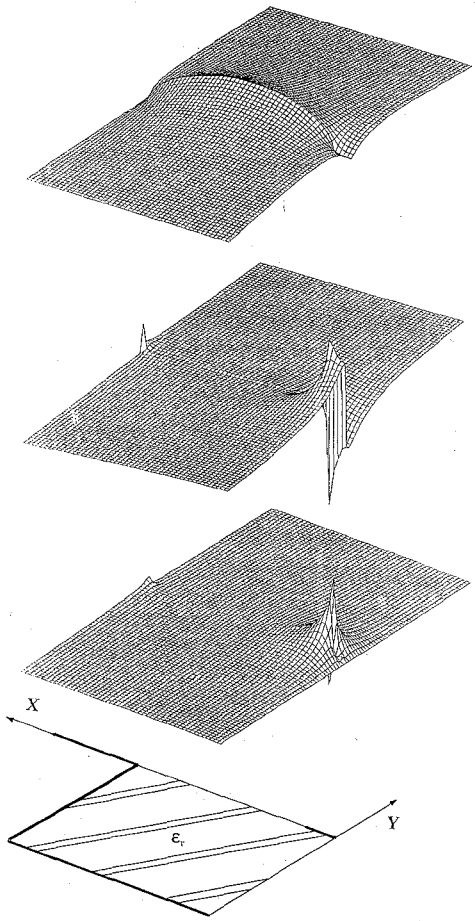

Fig. 4. E-field distribution in a cross section.

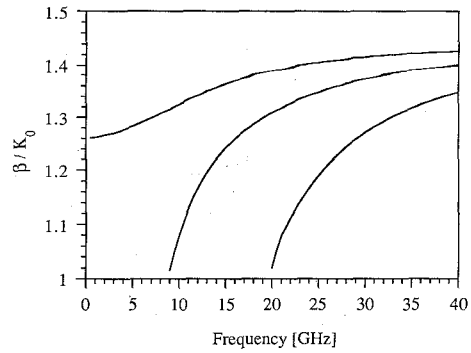

Fig. 5. Dispersion curves for the first three odd modes of mig.

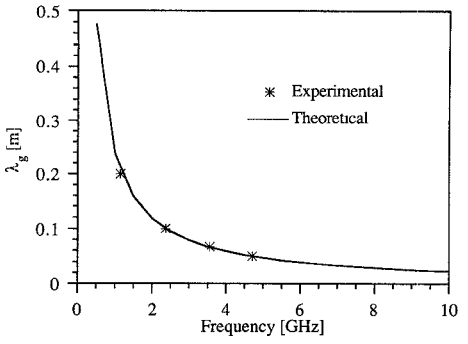

Fig. 6. Theoretical and experimental values of λ_g.

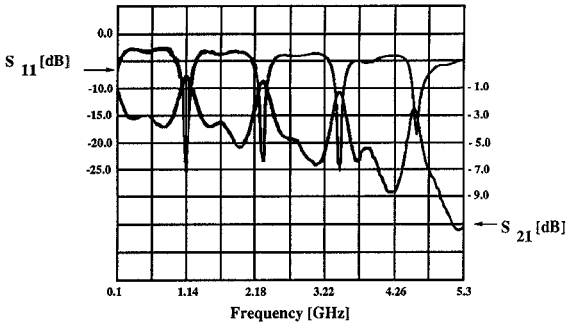

Fig. 7. Magnitude of $S11$ and $S21$ for a mig resonant cavity.

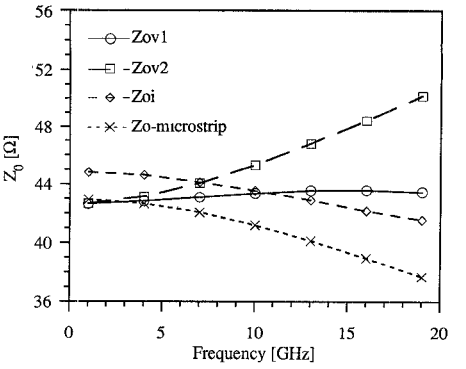

Fig. 8. Mig characteristic impedances versus frequency compared with the corresponding one of microstrip. (a = 5 mm; h = 0.5 mm; w = 2 mm).

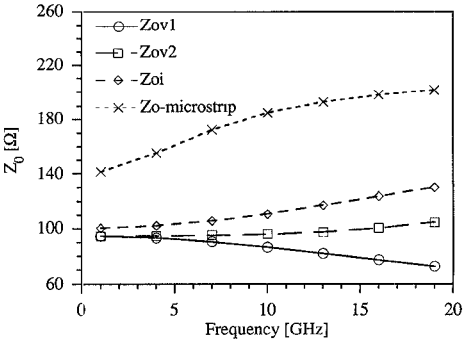

Fig. 9. Mig characteristic impedances versus frequency compared with the corresponding one of microstrip. (a = 5 mm; h = 5 mm; w = 2 mm).

where

$$V_1 = \int_{w/2}^{a/2} E_x(x, 0)\, dx = X_o N_o, \quad V_2 = \int_{-h}^{0} E_y(0, y)\, dy$$

and

$$I = \int_{-w/2}^{+w/2} H_x(x, 0^-)\, dx + \int_{-w/2}^{+w/2} H_x(x, 0^+)\, dx$$

$$P = \frac{1}{2} \iint_{\text{mig section}} (\mathbf{E} \times \mathbf{H}^*)\, d\mathbf{S}.$$

Figs. 8 and 9 show the impedance behavior vs frequency respectively for h = 0.5 mm and h = 5 mm [a = 5 mm, w = 2 mm]. A comparison with the corresponding curves for microstrip is particularly meaningful. It is seen that as h decreases, Z_o decreases as in microstrip. This is due to the fact that, when the height decreases ($h \ll a/2$), the capacitance between strip and side walls in negligible as compared to the capacitance between strip and the bottom of the groove. With regard to this, we note that an appreciable difference between parameters of mig and of microstrip exists when the ratio $\delta = (a - w/2h)$ is less than unity. In fact, in this case, the effect of the groove cannot be neglected.

In Fig. 8 we report a configuration for which δ = 3 where, in fact, the values of all impedances are close. On the contrary, in Fig. 9 the value of δ is 0.3 and there is an appreciable difference between the impedances of the different structures. Hence, from the global analysis of these and other results we can conclude that when $\delta \geq 1$, it is possible to use directly approximate formulas for microstrip [7], [8] to characterize mig without significant error. The same considerations can be made about the behavior of ϵ_{eff} (Table II).

Losses

Dielectric losses can be taken into account by using a complex value of the relative permittivity, ϵ_r, of the dielectric filling the groove and are found to be of the same order as the loss tangent (see [2]). Anyway, dielectric losses were found to be much lower than conduction losses. The latter were determined by the classical perturbation approach, as in [4].

Consequently, the power lost in the conductors per unit length of the guide is given by

$$P_c = \frac{R_m}{2} \int_C |\mathbf{J}|^2\, dl$$

$$= \frac{R_m}{2} \int_C (|(H_x|^2 + |H_y|^2 + |H_z|^2)\, dl \qquad (7)$$

where C is a path, in the mig transverse section, which includes all the conductors. The corresponding attenua-

TABLE II
COMPARISON OF $\sqrt{\epsilon_{\text{eff}}}$ BETWEEN mig (a = 5 mm; h = 0.5, 5 mm; w = 2 mm) AND MICROSTRIP (h = 0.5, 5 mm; w = 2 mm)

Frequency [GHz]	h = 0.5 mm mig	h = 0.5 mm microstrip	h = 5 mm mig	h = 5 mm microstrip
1.000	1.3462	1.3454	1.2635	1.2852
4.000	1.3472	1.3466	1.2651	1.3175
7.000	1.3489	1.3492	1.2679	1.3563
10.00	1.3510	1.3353	1.2715	1.3842
13.00	1.3534	1.3570	1.2759	1.4019
16.00	1.3560	1.3628	1.2810	1.4131
19.00	1.3589	1.3682	1.2865	1.4204

tion is given by

$$\alpha_c = \frac{1}{2}\frac{\text{energy dissipated by the conducting surface}}{\text{energy transmitted along the guide}} \cdot \left[\frac{\text{Np}}{\text{m}}\right] = \frac{P_c}{2P}\left[\frac{\text{Np}}{\text{m}}\right]. \quad (8)$$

The numerical difficulty that arises from the integration of a singular J_z on the strip-edge is overcome by considering a finite thickness of the strip conductor and modifying the edge behavior of the longitudinal current [4].

We assume the following current on the strip:

$$J_z(x) = J_o\left(1 - \left(\frac{2x}{w}\right)^2\right)^{-1/3}$$

and calculate J_o by imposing that the total longitudinal current on the strip be the same as in the ideal case of zero thickness:

$$\int_{\text{strip}} H_x(x)J_z(x)\,dx = \int_{\text{strip}} J_z(x)J_z(x)\,dx \quad (9)$$

from which, one derives

$$J_o = \int_{-w/2}^{+w/2} H_x(x)\left(1 - \left(\frac{2x}{w}\right)^2\right)^{-1/3} dx \Big/ \int_{-w/2}^{+w/2}\left(1 - \left(\frac{2x}{w}\right)^2\right)^{-2/3} dx \quad (10)$$

This approach proved numerically satisfactory, yielding an accurate lower limit to conduction losses.

Finally, conduction losses per unit length in Np/m are plotted separately in Fig. 10 versus dielectric thickness in the monomode range.

Losses for mig increase with the ratio w/h and they are of the same order of those of a microstrip.

Array Design

Having characterized the guiding structure, for the purpose of demonstrating feasibility, we designed a leaky-wave antenna. This antenna uses idg as guiding system and conducting strips, placed longitudinally on their air-dielectric interface, as radiating elements. This configuration ensures a very pure horizontal polarization for the

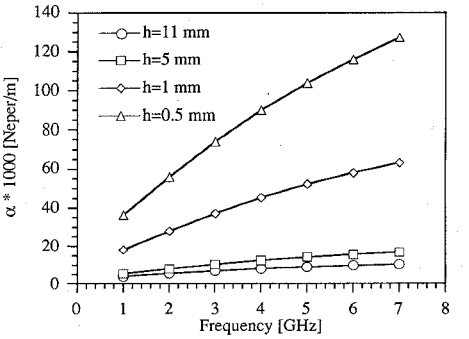

Fig. 10. Conduction losses versus frequency for various values of substrate thickness.

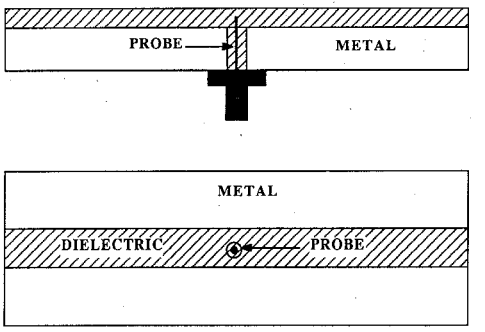

Fig. 11. Coaxial cable feeding.

antenna, due to an efficient coupling mechanism to the induced current on the strip in the z direction, while the current induced in the x direction is negligible. The strip lengths depend on feeding and current profile. We decided to feed the antenna by a coaxial cable principally for two reasons: 1) this feeding is easy to realize; 2) it makes the array design simple. In fact, if we feed the antenna centrally by introducing a probe in the dielectric substrate as in Fig. 11, we can use identical strips, obtaining a symmetric and smooth current profile. This ensures a good ratio between the main lobe and the secondary ones and a sufficiently narrow main lobe. This profile obtains thanks to the fact that, the farther the strips are from the center of the array, i.e., from the feeding point, the lower is the coupling to the traveling wave, as the preceding strips have already radiated some of the power. The lengths and spacing of the array elements are chosen so that $\lambda_g'/2$ long idg sections alternate with $\lambda_g''/2$ mig sections. In this manner, the total distance from the beginning of one strip to the beginning of the following one is $\lambda = \lambda_g'/2 + \lambda_g''/2$. Hence the induced currents on the strips are all in phase and a broadside array is obtained.

The prototype we realized is a 22 element horizontal array, operating at 10.0 GHz. Although, at this frequency, mig can operate in two modes, the resonance of the strips is essentially due to the fundamental mode and neglecting the second mode is unimportant for the design of the array. In Fig. 12 we report the radiation pattern of the antenna in the E-plane. It is noted that difference be-

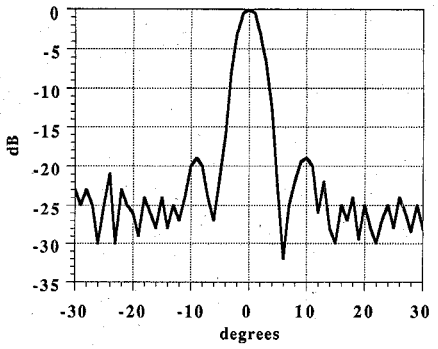

Fig. 12. Radiation pattern in the E-plane of a 22 elements array.

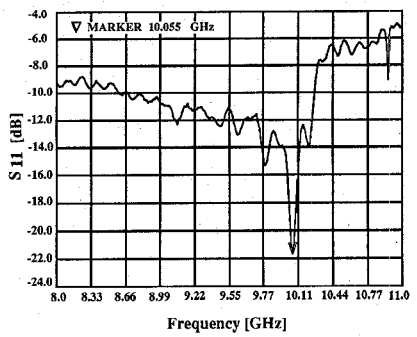

(a)

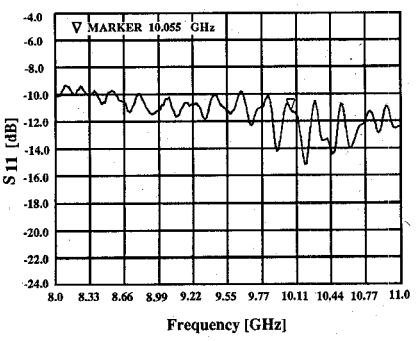

(b)

Fig. 13. Antenna reflection coefficient (a) compared with the idg one (b).

tween main lobe and side lobes is 18 dB. In Fig. 13 we also report the antenna reflection coefficient. It is interesting to note that although no special precautions were taken, input reflection was below -20 dB at the central frequency.

IV. Conclusion

We analyzed the waveguiding properties of mig, including hybrid modes, characteristic impedance and losses.

Its fundamental mode characteristic are not dissimilar to those of microstrip: its main advantage lies in the presence of two conductors on the accessible interface, as in coplanar guide, but without the risk of surface wave excitation.

As a practical application we realized a 22-elements, centrally fed, horizontally polarized array, alternating $\lambda_g/2$ sections of mig and empty idg. Experimental antenna characteristics show good input match, efficiency, gain and polarization properties. This feasibility study demonstrates how mig is a natural choice for integrated feeds and antenna media.

Appendix

The complete expression of the Fourier coefficients are

$$P_i(k_x) = \int_{w/2}^{a/2} \frac{dx}{\sqrt{\left(\frac{2x}{w} - 1\right)}\sqrt[3]{1 - \left(\frac{2x}{a}\right)}} \cdot \sqrt{\frac{2}{\pi}} \sin(k_x x) f_i(x)$$

$$= \sqrt{\frac{2}{\pi}} \left(\frac{a-w}{w}\right)^{-1/2} \left(\frac{a-w}{a}\right)^{-1/3} \left(\frac{a-w}{2}\right) \cdot \sqrt{\frac{(2i + 1/6)\Gamma(1/2 + i)}{i!\,\Gamma(1/6 + i + 1/2)}} A\left(i, k_x \frac{a-w}{2}, w\right)$$

$$P_{in} = \int_{w/2}^{a/2} \frac{dx}{\sqrt{\left(\frac{2x}{w} - 1\right)}\sqrt[3]{1 - \left(\frac{2x}{a}\right)}} \frac{2}{\sqrt{a}} \cdot \sin\left(\frac{n\pi}{a} x\right) f_i(x)$$

$$= \frac{2}{\sqrt{a}} \left(\frac{a-w}{w}\right)^{-1/2} \left(\frac{a-w}{a}\right)^{-1/3} \left(\frac{a-w}{2}\right) \cdot \sqrt{\frac{(2i + 1/6)\Gamma(1/2 + i)}{i!\,\Gamma(1/6 + i)\Gamma(1/6 + i + 1/2)}} \cdot A\left(i, \frac{n\pi}{a} \frac{a-w}{2}, w\right)$$

where

$$A(i, z, w) = \sum_{m=0,1}^{i} (-1)^m \binom{i}{m} \frac{\Gamma(1/6 + 2i - m)}{2\Gamma(1/2 + i - m)} \cdot \left\{ -jB(2/3, i - m + 1/2) \cos\frac{zw}{2} \cdot I_-(i, m, z) + B(2/3, i - m + 1/2) \cdot \sin\frac{zw}{2} I_+(i, m, z) \right\}$$

and

$$I_{\pm}(i, m, z) = [M(i - m + 1/2; i - m + 1/2 + 2/3; jz) \pm M(i - m + 1/2; i - m + 1/2 + 2/3; -jz)].$$

B and Γ are respectively the Beta function and the Gamma function; M is the Kummer function or degenerate hypergeometric function. The explicit expressions for M can be found in [5, p. 504] as series of alternating terms. This series converges rapidly for small values of $|z|$ ($|z| < 10$). For greater values of $|z|$ the previous series becomes numerically unmanageable so that it is necessary to take the asymptotic expansion [5, p. 508] of the Kummer function. The final expressions of the functions $I_{\pm}(i, m, z)$ are for $|z| < 4$

$$I_{+}(i, m, z) = 2 \sum_{k=0,2}^{\infty} \frac{(z)^k}{k!} (-1)^{k/2} \frac{(i - m + 1/2)_k}{(i - m + 7/6)_k}$$

$$I_{-}(i, m, z) = 2j \sum_{k=1,3}^{\infty} \frac{(z)^k}{k!} (-1)^{(k-1)/2} \frac{(i - m + 1/2)_k}{(i - m + 7/6)_k}$$

and for $|z| > 4$

$$I_{+}(i, m, z) = 2\Gamma(i - m + 7/6) \left\{ \frac{(z)^{-(i-m+0.5)}}{\Gamma(2/3)} \sum_{k=0,1}^{R-1} z^{-k} \cdot \frac{(i - m + 1/2)_k (1/3)_k}{k!} \cdot \cos\left(\frac{\pi}{2}(i - m + 1/2 + k)\right) + \frac{(z)^{-(2/3)}}{\Gamma(i - m + 0.5)} \sum_{k=0,1}^{S-1} z^{-k} \cdot \frac{(1/2 - i + m)_k (2/3)_k}{k!} \cdot \cos\left(z - \frac{\pi}{2}(2/3 + k)\right) \right\}$$

$$I_{-}(i, m, z) = 2j\Gamma(i - m + 7/6) \left\{ \frac{(z)^{-(i-m+0.5)}}{\Gamma(2/3)} \sum_{k=0,1}^{R-1} \cdot z^{-k} \frac{(i - m + 1/2)_k (1/3)_k}{k!} \cdot \sin\left(\frac{\pi}{2}(i - m + 1/2 + k)\right) + \frac{(z)^{-(2/3)}}{\Gamma(i - m + 0.5)} \sum_{k=0,1}^{S-1} z^{-k} \cdot \frac{(1/2 - i + m)_k (2/3)_k}{k!} \cdot \sin\left(z - \frac{\pi}{2}(2/3 + k)\right) \right\}$$

The errors committed in the asymptotic approximations of Kummer functions are of order $O(z^{-R})$ and $O(z^{-S})$, so that three terms for each series are sufficient to represent correctly $I_{\pm}$.

References

[1] T. Rozzi, R. De Leo, and A. Morini, "Analysis of the microstrip-loaded inset dielectric waveguide," *1989 IEEE MTT's Int. Microwave Symp. Dig.*, pp. 923–926.

[2] T. Rozzi and S. Hedges, "Rigorous analysis and network modelling of the Inset Dielectric Guide," *IEEE Trans. Microwave Theory Tech.*, vol. MTT-35, Sept. 1987.

[3] T. Rozzi, A. De Leo, L. Ma, A. Morini, "Equivalent network of transverse dipoles on inset dielectric guide: application to linear array," *IEEE Trans. Antennas Propagat.*, vol. 38, Mar. 1990.

[4] T. Rozzi, F. Moglie, A. Morini, E. Marchionna, and M. Politi, "Hybrid modes, substrate leakage and losses of slotline at millimeter wave frequencies," *IEEE Trans. Microwave Theory Tech.*, August 1990.

[5] I. Abramovitz and I. A. Stegun, *Handbook of Mathematical Functions*. New York: Dover, Inc., 1970.

[6] I. S. Gradshteyn and I. M. Ryzhik, *Table of Integrals, Series and Products*. New York: Academic, 1965.

[7] J. C. Gupta *et al.*, *Microstrip Line and Slotline*. Norwood, MA: Artech House, 1979.

[8] Bianco *et al.*, "Frequency dependence of microstrip parameters," *Alta Frequenza* vol. XLIII, no. 7, July 1974.

Tullio Rozzi (M'66–SM'74–F'90) was born in Italy in 1941. He received the degree of "dottore" in physics from Pisa University Italy in 1965, the Ph.D. degree in electrical engineering from Leeds University, U.K., in 1968 and the D.Sc. degree from the University of Bath, U.K., in 1987.

From 1968 to 1978 he was a Research Scientist at the Philips Research Laboratories, Eindhoven, The Netherlands, having spent one year, 1975, at the Antenna Laboratory, University of Illinois, Urbana. In 1978 he was appointed to Chair of Electrical Engineering at University of Liverpool, U.K., and subsequently was appointed to the Chair of Electronics and Head of the Electronics Group at the University of Bath in 1981. From 1983 to 1986 he held the additional responsibility of Head of School of Electrical Engineering at Bath. Since 1986 he has held the Chair of Antennas at the Faculty of Engineering, University of Ancona, Ancona, Italy.

In 1975 Dr. Rozzi was awarded the Microwave Prize by the IEEE Microwave Theory and Techniques Society. He is also a Fellow of the IEE (U.K.).

Antonio Morini was born in Italy in 1962. He received the degree in electronic engineering from the University of Ancona, Ancona, Italy, in 1987.

Since 1988 he has been with the Department of Electronics and Automatics at the University of Ancona as a Research Assistant. His research is mainly devoted to the modeling of passive millimetric wave devices and antennas.

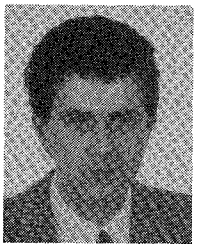

Giampiero Gerini received the "laurea" degree in electronic engineering from the University of Ancona, Ancona, Italy, in 1988. He is presently pursuing the Ph.D. degree in electromagnetic fields and circuits in the Department of Electronics and Automatics at the University of Ancona.

His research is mainly devoted to the study of passive millimetric wave devices and antennas, within the general area of applied electromagnetics.